

SP²OT: Semantic-Regularized Progressive Partial Optimal Transport for Imbalanced Clustering

Chuyu Zhang, Hui Ren, and Xuming He

Abstract—Deep clustering, which learns representation and semantic clustering without labels information, poses a great challenge for deep learning-based approaches. Despite significant progress in recent years, most existing methods focus on uniformly distributed datasets, significantly limiting the practical applicability of their methods. In this paper, we propose a more practical problem setting named deep imbalanced clustering, where the underlying classes exhibit an imbalance distribution. To address this challenge, we introduce a novel optimal transport-based pseudo-label learning framework. Our framework formulates pseudo-label generation as a Semantic-regularized Progressive Partial Optimal Transport (SP²OT) problem, which progressively transports each sample to imbalanced clusters under several prior distribution and semantic relation constraints, thus generating high-quality and imbalance-aware pseudo-labels. To solve SP²OT, we develop a Majorization-Minimization-based optimization algorithm. To be more precise, we employ the strategy of majorization to reformulate the SP²OT problem into a Progressive Partial Optimal Transport problem, which can be transformed into an unbalanced optimal transport problem with augmented constraints and can be solved efficiently by a fast matrix scaling algorithm. Experiments on various datasets, including a human-curated long-tailed CIFAR100, challenging ImageNet-R, and large-scale subsets of fine-grained iNaturalist2018 datasets, demonstrate the superiority of our method. Code is available: <https://github.com/rhfeiyang/SPPOT>.

Index Terms—Deep Clustering, Optimal Transport, Imbalanced Clustering



arXiv:2404.03446v1 [cs.CV] 4 Apr 2024

1 INTRODUCTION

Humans possess an inherent ability to categorize similar concepts, even when encountering them for the first time. However, artificial models face challenges in grouping similar concepts without explicit labels, highlighting the limitations of traditional supervised learning approaches. Recognizing this gap, the field of deep clustering has emerged as a promising avenue. Deep clustering goes beyond supervised learning approaches by simultaneously learning effective representations and semantic clustering, enabling models to discern and group similar concepts in an unsupervised manner. Several seminal works, including [1], [2], [3], have made significant contributions to advancing the field of deep clustering. However, a prevalent limitation in existing research lies in its emphasis on developing methods tailored for balanced datasets. While these approaches showcase promising results in controlled environments, their practical applicability is restricted due to prevalent imbalanced data distributions in real-world scenarios. Consequently, there is a growing need to extend the capabilities of deep clustering methods to handle imbalanced datasets effectively, ensuring their robust performance across a broader spectrum of real-world applications.

In this paper, we consider a practical deep imbalanced clustering problem, bridging the gap between existing deep clustering methodologies and realistic settings. Current approaches can be broadly classified into three categories: relation matching-based [4], mutual information maximization-based [1], and pseudo-labeling-based [2] methods. They face significant challenges when dealing with imbalanced clustering. Specifically, relation matching and mutual information maximization-based methods adopt surrogate losses for clustering and disregard imbalanced cluster distributions, potentially leading to subpar outcomes in imbalanced scenarios [5], [6]. Pseudo-labeling suffers from three drawbacks in deep imbalanced clustering. Firstly, it heavily depends on the assumption of a uniform distribution, which causes it to fail in handling imbalanced scenarios, an issue explored in Sec. 6.2.1. Secondly, it usually necessitates an additional phase for initializing representations [2], [7] and requires tedious hyperparameter calibration to alleviate confirmation bias [8]. Lastly, it primarily generates pseudo-labels by utilizing information in the label space without any adjustment. Consequently, this approach is prone to bias in imbalanced scenarios [9] and fails to leverage the rich semantic information inherent in the representation space.

To mitigate the aforementioned weaknesses, we introduce a novel progressive learning framework based on pseudo-labeling. This framework formulates the pseudo-label generation as a Semantic-regularized Progressive Partial Optimal Transport (SP²OT) algorithm. This SP²OT seamlessly integrates three critical components into a unified optimal transport (OT) problem: K-Nearest-Neighbor (KNN) graph-based semantic relation regularization, modeling of imbalanced

- Chuyu Zhang is with the ShanghaiTech University and Lingang Laboratory, Shanghai, 201210, China. E-mail: zhangchy2@shanghaitech.edu.cn
- Hui Ren is with the ShanghaiTech University, Shanghai 201210, China. E-mail: renhui@shanghaitech.edu.cn
- Xuming He is with the ShanghaiTech University and Shanghai Engineering Research Center of Intelligent Vision and Imaging, Pudong, Shanghai 201210, China. E-mail: hexm@shanghaitech.edu.cn

Manuscript received April 19, 2024; revised August 26, 2015.

class distributions, and the selection of confident samples. This novel integration empowers our algorithm to generate high-quality and imbalanced pseudo-labels by considering both the output and semantic space simultaneously, while alleviating confirmation bias through progressive learning from high-confidence samples. In addition, we develop an efficient Majorization-Minimization (MM) algorithm-based solver for the proposed SP²OT problem.

Specifically, our framework performs clustering by generating pseudo-labels and learning from them alternately. We formulate the pseudo-label generation as the SP²OT algorithm, which assigns each sample to clusters with minimal cost. The transportation cost is defined as the negative log of model predictions, and the assignment is subject to constraints on sample relations in the representation space and a set of prior constraints. The key constraints in our formulation are: 1) Distribution Constraint: We employ a Kullback-Leibler (KL) divergence constraint to ensure a uniform distribution of cluster sizes. This constraint is crucial for preventing degenerate solutions while allowing for the generation of imbalanced pseudo-labels due to its relaxed nature compared to an equality constraint. 2) Total Mass Constraint: By adjusting sample weights through optimization, the total mass constraint enables selective learning from high-confidence samples. This mitigates the impact of noisy pseudo-labels and eliminates the need for sensitive hand-crafted confidence threshold tuning. Moreover, incrementally raising the total mass constraint facilitates a gradual transition from learning easy samples to tackling more challenging ones. 3) Semantic Relation Regularization: We incorporate a semantic relation regularization term represented by a K-Nearest Neighbor (KNN) graph. This regularization ensures that similar pseudo-labels are generated for the nearest samples in the representation space, enhancing the overall quality of the pseudo-labels.

In addition, to solve SP²OT, we devise a novel iterative optimization approach based on the MM algorithm. Initially, we leverage the Taylor expansion to construct an upper bound of SP²OT and manifest the upper bound as a Progressive Partial Optimal Transport (P²OT) [10] problem. To solve P²OT efficiently, we introduce a virtual cluster and replace the conventional KL divergence with a weighted KL constraint. Then reformulate P²OT into an unbalanced optimal transport problem, which can be solved by an efficient scaling algorithm and relies solely on matrix-vector multiplications.

In contrast to the earlier conference version [10], which relies solely on output space for pseudo-label generation, SP²OT introduces an innovative semantic regularization based on a KNN graph (Sec.4.3). Furthermore, we have devised a novel solver in Sec.5.2.1 based on the MM algorithm, specifically crafted to address SP²OT.

To validate our method, we conduct experiments on a wide range of challenging datasets, including the human-curated CIFAR100 dataset [11], challenging ‘out-of-distribution’ ImageNet-R dataset [12], and large-scale subsets of fine-grained iNaturalist18 dataset [13]. Experiments on those challenging datasets demonstrate the effectiveness of each component and the superiority of our method.

In summary, our contribution is as follows:

- We generalize the deep clustering problem to more realistic imbalance scenarios, and establish a new benchmark.
- We introduce a pseudo-label learning framework for deep imbalance clustering, along with a novel SP²OT algorithm. This approach enables us to effectively account for semantic relations, class imbalance distribution, and progressive learning during pseudo-label generation.
- We propose a solver based on the MM algorithm for the novel SP²OT. Specifically, we derive the upper bound of SP²OT, reformulate the upper bound as an unbalanced OT problem with a theoretical guarantee, and solve it with the efficient scaling algorithm.
- Our method achieves the SOTA performance on most datasets compared with existing methods on our newly proposed challenging and large-scale benchmark.

2 RELATED WORK

2.1 Deep clustering

The goal of deep clustering [14], [15] is to learn representation and cluster data into semantic classes simultaneously. Based on clustering methods, current works can be grouped into three categories: relation matching, mutual information maximization, and pseudo labeling. Specifically, relation matching [2], [16], [17] involves the minimization of the distance between instances considered ‘similar’ by representation distance, thus achieving clustering in a bottom-up way. Mutual information maximization [1], [18], [19] either in the prediction or representation space, aims at learning invariant representations for images with different augmentation, thereby achieving clustering implicitly [20]. Pseudo labeling (PL) [21], which is the focus of this paper and widely used in semi-supervised learning [22], [23], assigns each instance to semantic clusters and has demonstrated exceptional performance in the domain of deep clustering [2], [7], [24], [25]. In contrast to the relatively clean pseudo-labels produced by semi-supervised learning, deep clustering often generates noisier pseudo-labels, particularly in scenarios characterized by data imbalance, imposing a great challenge on pseudo-label generation.

To acquire high-quality pseudo labels, [2], [7] often need multiple-stage training and meticulous manual selection of confidence samples. Specifically, Van *et al.* [2] initially focuses on learning clustering by minimizing the distance between similar images. Subsequently, they undertake confidence sample selection employing hand-crafted thresholding, with variations tailored to different datasets. Based on the unrealistic uniform assumption, Niu *et al.* [7] select an equal number of reliable samples for each class based on the confidence ratio and apply FixMatch-like training in the third training stage, which usually fails in the imbalance scenarios.

By contrast, instead of relying on the strong uniform distribution constraint and manual sample selection, our PL-based SP²OT algorithm progressively generates high-quality pseudo labels by simultaneously considering class imbalance distribution, sample confidence, and semantic regularization through a single convex optimization problem.

2.2 Self-supervised Learning

Self-supervised Learning (SSL) [26], [27] aims to learn meaningful representation from vast unlabeled data. In our

perspective, SSL methodologies can be broadly categorized into three groups: contrastive learning [28], [29], [30], [31], self-distillation [32], [33], [34], and reconstruction-based [35], [36], [37] approaches. Contrastive learning methods operate on the principle of encouraging similarity between semantically transformed versions of an input. Self-distillation methods focus on learning invariant predictions from different views while avoiding collapsing through variant techniques. Reconstruction-based methods, on the other hand, aim to predict the original image through generative models or masked image modeling. For a more comprehensive exploration of these SSL methods, we direct the reader to [38]. It is noteworthy that these SSL techniques can be used as a robust foundational model for deep clustering.

In SSL, the works mostly related to us are [5], [6], [39], which aim to learn representation from imbalanced data. To defend the bias introduced by imbalanced data, Jiang *et al.* [5] propose self-damaging contrastive learning to emphasize the most easily forgotten samples, Liu *et al.* [39] devise a re-weighted regularization technique based on theoretical insights, and Zhou *et al.* [6] leverages the memorization effect of deep neural networks to automatically drive the information discrepancy of the sample views in contrastive learning. In contrast to these methodologies, our approach involves simultaneous representation learning through pseudo-labeling and the acquisition of cluster heads from imbalanced data.

2.3 Supervised Long-tailed Learning

Supervised long-tailed learning [40], [41] is designed to acquire unbiased representations and classifiers from datasets with imbalanced class distributions. Various methods have been proposed to enhance the learning of tail classes by leveraging information about the known class distribution. For instance, Logit Adjustment [42] addresses classifier bias by adjusting the logits based on class frequencies. Kang *et al.* [9] take a different approach by decoupling representation and classifier learning. They first learn representations through instance-balanced resampling and then retrain classifiers using re-balancing techniques. For a more extensive survey, readers are encouraged to refer to [43]. In contrast to supervised long-tailed learning, deep imbalanced clustering faces the challenge of dealing with an unknown and imbalanced distribution, rendering the aforementioned techniques challenging to apply.

2.4 Optimal transport and its application

Optimal Transport (OT) [44], [45], [46], [47], [48] aims to find the most efficient transportation plan while adhering to marginal distribution constraints. It has been used in a broad spectrum of machine learning tasks, including but not limited to generative model [49], [50], semi-supervised learning [51], [52], clustering [25], [53], domain adaptation [54], [55], [56], [57] and others [58], [59]. Of particular relevance to our work is its utilization in pseudo labeling [25], [51], [60]. Compared to naive pseudo labeling [21], OT can consider class distribution to generate high-quality pseudo labels and avoid the degenerate solution. Specifically, Asano *et al.* [25] initially introduces an equality constraint on cluster size, formulating pseudo-label generation as an optimal transport problem. Subsequently, Tai *et al.* [51] enhances the

flexibility of optimal transport by incorporating relaxation on the constraint, which results in its failure in deep imbalanced clustering, and introduces label annealing strategies through an additional total mass constraint. Recently, Zhang *et al.* [60] relaxes the equality constraint to a KL divergence constraint on cluster size, thereby addressing imbalanced data scenarios. In contrast to these approaches, which either ignore class imbalance distribution or the confidence of samples, our SP²OT algorithm takes both into account simultaneously, allowing us to generate pseudo-labels progressively and with an awareness of class imbalance. In terms of computational efficiency, we solve our SP²OT by the Majorization-Minimization algorithm, then transform the inner optimization problem into an unbalanced optimal transport problem under specific constraints and utilize a light-speed scaling algorithm.

3 PRELIMINARY

Optimal Transport (OT) tackles the general problem of moving one distribution of mass to another with minimal cost. Mathematically, given two probability vectors $\boldsymbol{\mu} \in \mathbb{R}^{m \times 1}$, $\boldsymbol{\nu} \in \mathbb{R}^{n \times 1}$, as well as a cost matrix $\mathbf{C} \in \mathbb{R}^{m \times n}$ defined on joint space, the objective function which OT minimizes is as follows:

$$\min_{\mathbf{Q} \in \mathbb{R}^{m \times n}} \langle \mathbf{Q}, \mathbf{C} \rangle_F + F_1(\mathbf{Q}\mathbf{1}_n, \boldsymbol{\mu}) + F_2(\mathbf{Q}^\top \mathbf{1}_m, \boldsymbol{\nu}) \quad (1)$$

where $\mathbf{Q} \in \mathbb{R}^{m \times n}$ is the transportation plan, $\langle \cdot, \cdot \rangle_F$ denotes the Frobenius product, F_1, F_2 are constraints on the marginal distribution of \mathbf{Q} and $\mathbf{1}_n \in \mathbb{R}^{n \times 1}$, $\mathbf{1}_m \in \mathbb{R}^{m \times 1}$ are all ones vector. For example, if F_1, F_2 are equality constraints, i.e. $\mathbf{Q}\mathbf{1}_n = \boldsymbol{\mu}$, $\mathbf{Q}^\top \mathbf{1}_m = \boldsymbol{\nu}$, the above OT becomes a widely-known Kantorovich's form [61]. And if F_1, F_2 are KL divergence or inequality constraints, Eq.(1) turns into the unbalanced OT problem [62].

In practice, to efficiently solve Kantorovich's form OT problem, Cuturi [63] introduces an entropy term $-\epsilon \mathcal{H}(\mathbf{Q})$ to Eq.(1) and solve the entropic regularized OT with the efficient scaling algorithm [64]. Subsequently, Chizat *et al.* [65] generalizes the scaling algorithm to solve the unbalanced OT problem. Therefore, Eq.(1) can be solved by Algorithm 1. We show more detail of the scaling algorithm in the Appendix 2. Additionally, one can introduce the total mass constraint to Eq.(1), and it can be solved by the efficient scaling algorithm by adding a dummy or virtual point to absorb the total mass constraint into marginal.

Recently, Asano *et al.* [25] applied optimal transport to generate pseudo labels for unsupervised clustering. Specifically, given the model's prediction and its pseudo-label, the loss function is denoted as follows:

$$\mathcal{L} = - \sum_{i=1}^N \mathbf{Q}_i \log \mathbf{P}_i = \langle \mathbf{Q}, -\log \mathbf{P} \rangle_F, \quad (2)$$

where $\langle \cdot, \cdot \rangle_F$ is the Frobenius product, $\mathbf{Q}, \mathbf{P} \in \mathbb{R}_+^{N \times K}$, $\mathbf{Q}_i, \mathbf{P}_i$ is the pseudo label and prediction of sample x_i . Note that we have absorbed the normalize term $\frac{1}{N}$ into \mathbf{Q} for simplicity, thus $\mathbf{Q}\mathbf{1}_K = \frac{1}{N}\mathbf{1}_N$.

By making the assumption of equal distribution within the cluster, Asano *et al.* [25] approach the problem of pseudo-

Algorithm 1: Scaling Algorithm for OT

Input: Cost matrix \mathbf{C} , ϵ , m , n , $\boldsymbol{\mu}$, $\boldsymbol{\nu}$
 $\mathbf{M} = \exp(-\mathbf{C}/\epsilon)$
 $\mathbf{b} \leftarrow \mathbf{1}_n$
while \mathbf{b} *not converge* **do**
 $\mathbf{a} \leftarrow \text{prox}_{F_1/\epsilon}^{KL}(\mathbf{M}\mathbf{b}, \boldsymbol{\mu})/(\mathbf{M}\mathbf{b})$
 $\mathbf{b} \leftarrow \text{prox}_{F_2/\epsilon}^{KL}(\mathbf{M}^\top \mathbf{a}, \boldsymbol{\nu})/(\mathbf{M}^\top \mathbf{a})$
end
return $\text{diag}(\mathbf{a})\mathbf{M}\text{diag}(\mathbf{b})$

label generation by formulating it as an optimal transport problem, as expressed by the following formulation:

$$\min_{\mathbf{Q} \in \Pi} \langle \mathbf{Q}, -\log \mathbf{P} \rangle_F \quad (3)$$

$$\text{s.t. } \Pi = \{ \mathbf{Q} \in \mathbb{R}_+^{N \times K} \mid \mathbf{Q}\mathbf{1}_K = \frac{1}{N}\mathbf{1}_N, \mathbf{Q}^\top \mathbf{1}_N = \frac{1}{K}\mathbf{1}_K \} \quad (4)$$

where λ is a scalar factor. Intuitively, Π in Eq.(4) transports each data point to uniformly distributed clusters with minimal cost based on the distance between the sample and cluster. The authors then employ the Algorithm 1, to obtain the optimal \mathbf{Q}^* . Subsequently, utilizing \mathbf{Q}^* , the model is updated using Eq.(2). Interestingly, the clustering is achieved through iterative optimization of Eq.(3) and Eq.(2), both sharing the same objective. Our algorithm builds upon this formulation, deviating from the balanced cluster assumption and incorporating additional semantic constraints. This modification enhances the algorithm’s performance and makes it applicable to more realistic scenarios where the cluster is imbalanced.

4 METHOD

4.1 Problem Setup and Method Overview

In deep imbalanced clustering, the training dataset is denoted as $\mathcal{D} = \{(x_i)\}_{i=1}^N$, where the cluster labels and distribution are unknown. The number of clusters K is predefined by the user or estimated by other methods. The goal is to learn representation and semantic clusters. To achieve that, we learn representation and generate pseudo-label alternately, improving the data representation and the quality of cluster assignments. Specifically, given the cluster prediction, we utilize our novel Semantic-regularized Progressive Partial Optimal Transport (SP²OT) algorithm to generate high-quality pseudo labels. Our SP²OT algorithm has three advantages: 1) generating pseudo labels in an imbalanced manner; 2) reweighting confident samples through optimization; and 3) incorporating semantic information as a regularization. Then, given the pseudo label, we update the representation. We alternate the above two steps until convergence.

To provide a comprehensive understanding of our innovative SP²OT algorithm, we begin by deriving the formulation of the P²OT algorithm, which serves as a foundational component without considering the semantic constraint present in SP²OT. Then, we meticulously outline the semantic constraint, leveraging it in conjunction with P²OT to derive the SP²OT algorithm.

4.2 Progressive Partial Optimal Transport (P²OT)

In deep clustering, it is typical to impose some constraint on the cluster size distribution to avoid a degenerate solution,

where all the samples are assigned to a single cluster. As the cluster distribution is long-tailed and unknown, we adopt a KL divergence constraint and only assume the prior distribution is uniform. Therefore, with two marginal distribution constraints, we can formulate the pseudo-label generation problem as an unbalanced OT problem:

$$\min_{\mathbf{Q} \in \Pi} \langle \mathbf{Q}, -\log \mathbf{P} \rangle_F + \lambda KL(\mathbf{Q}^\top \mathbf{1}_N, \frac{1}{K}\mathbf{1}_K) \quad (5)$$

$$\text{s.t. } \Pi = \{ \mathbf{Q} \in \mathbb{R}_+^{N \times K} \mid \mathbf{Q}\mathbf{1}_K = \frac{1}{N}\mathbf{1}_N \} \quad (6)$$

where $\langle \cdot, \cdot \rangle_F$ is the Frobenius product, and λ is a scalar factor. In Eq.(5), the first term is exactly \mathcal{L} , the KL term is a constraint on cluster size, and the equality term ensures each sample is equally important.

However, the unbalanced OT algorithm treats each sample equally, which may generate noisy pseudo labels, due to the initial representation being poor, resulting in confirmation bias. Inspired by curriculum learning [66], which first learns from easy samples and gradually learns hard samples, we select only a fraction of high-confident samples to learn initially and increase the fraction gradually. However, instead of manually selecting confident samples through sensitive thresholding, we formulate the selection process as a total mass constraint in Eq.(7). This approach allows us to reweight each sample through joint optimization with the pseudo-label generation, eliminating the need for sensitive hyperparameter tuning. Therefore, the formulation of our novel P²OT is as follows:

$$\min_{\mathbf{Q} \in \Pi} \langle \mathbf{Q}, -\log \mathbf{P} \rangle_F + \lambda KL(\mathbf{Q}^\top \mathbf{1}_N, \frac{\rho}{K}\mathbf{1}_K) \quad (7)$$

$$\text{s.t. } \Pi = \{ \mathbf{Q} \in \mathbb{R}_+^{N \times K} \mid \mathbf{Q}\mathbf{1}_K \leq \frac{1}{N}\mathbf{1}_N, \mathbf{1}_N^\top \mathbf{Q}\mathbf{1}_K = \rho \} \quad (8)$$

where ρ is the fraction of selected mass and will increase gradually, and KL is the unnormalized divergence measure, enabling us to handle imbalance distribution. Under the total mass constraint, the algorithm prioritizes moving samples with minimal cost (higher \mathbf{P}) to each cluster, achieving high-confidence sample selection. The resulting $\mathbf{Q}\mathbf{1}_K$ represents the weights for samples, and we directly utilize it to reweight each sample without any further modification. Intuitively, P²OT encompasses a set of prior distribution constraints, achieving the generation of imbalanced pseudo-labels through a relaxed KL constraint and reweighting confident samples by total mass constraint within a single optimization problem.

4.3 Semantic constraint

By now, our algorithm is able to generate pseudo-labels solely based on the model’s predictions in the output space. However, it is noteworthy that the model’s predictions may lack reliability, particularly during the early stages of training, and it tends to bias to head classes in imbalanced scenarios [42]. On the other hand, the proposed P²OT only considers the point-wise prediction and statistical distribution constraints to generate pseudo-labels, which ignores the valuable semantic relation among samples, resulting in sub-optimal outcomes.

To address the issues mentioned, we propose incorporating the semantic information obtained from the feature space

of the pre-trained model backbone, which is more robust to imbalanced data, into the pseudo-label generation process. Specifically, given the feature representation of all samples in the dataset $\mathbf{z} = \{z_1, \dots, z_N\} \in \mathbb{R}^{N \times D}$, we construct a K-Nearest Neighbor Graph (K-NNG) to capture reliable and meaningful semantic relations, such as manifold structures among samples. Where the adjacency matrix $\mathbf{A} \in \mathbb{R}^{N \times N}$ is defined as follows:

$$\mathbf{S} : \mathbf{S}_{i,j} = K(z_i, z_j) = \exp\left(-\frac{\|z_i - z_j\|^2}{2\sigma^2}\right) \quad (9)$$

$$\mathbf{A} = F(\mathbf{S}), \quad (10)$$

where K is a Gaussian kernel function and \mathbf{S} is similarity gram matrix. F is the operation of setting the diagonal and non-topk elements of the gram matrix to 0, i.e. we select k nearest neighbors in the whole dataset for each sample.

Ensuring the reliability of semantic information necessitates obtaining a high-quality feature representation, denoted as \mathbf{z} . While a straightforward approach involves extracting this representation from the model backbone online during training, our observations reveal that, particularly in the early stages of training, suboptimal classifiers can introduce noise during backbone updating. This noise can lead the model to learn in inappropriate directions, causing a degradation in feature quality throughout training. To address this issue, we propose obtaining the feature representation from the initial pre-trained model backbone. This approach not only mitigates the problem but also reduces training time costs, as it necessitates computing the adjacency matrix only once at the start, as opposed to the ongoing construction of the K-NNG during training.

Then, we utilize the adjacency matrix \mathbf{A} as a semantic regularization term. Intuitively, our goal is for samples with close proximity in the feature space also to exhibit low distances in the output and label spaces. The final formulation of our semantic-regularized progressive partial optimal transport is as follows:

$$\min_{\mathbf{Q} \in \Pi} \langle \mathbf{Q}, -\log \mathbf{P} \rangle_F - \lambda_1 \langle \mathbf{A}, \mathbf{Q} \mathbf{Q}^\top \rangle_F + \lambda_2 KL(\mathbf{Q}^\top \mathbf{1}_N, \frac{\rho}{K} \mathbf{1}_K) \quad (11)$$

$$\text{s.t. } \Pi = \{\mathbf{Q} \in \mathbb{R}_+^{N \times K} | \mathbf{Q} \mathbf{1}_K \leq \frac{1}{N} \mathbf{1}_N, \mathbf{1}_N^\top \mathbf{Q} \mathbf{1}_K = \rho\}, \quad (12)$$

where λ_1 is the regulation factor for semantic regularization. We let λ_1 decay with the training process in our implementation. The information from model prediction gradually becomes reliable, while the semantic information is from the initial pre-trained model backbone, which will be less informative and may limit the model's flexibility. Specifically, we reuse ρ , which increases with the training progress and will be illustrated in Sec.5.1, to decay λ_1 :

$$\lambda_1 = \lambda_1^0 \cdot (1 - \rho), \quad (13)$$

where λ_1^0 is the initial value of λ_1 .

5 TRAINING

To train our model, we initially generate pseudo-labels using our novel SP²OT algorithm and subsequently utilize these pseudo-labels to supervise the model learning process. Moreover, inspired by curriculum learning, we progressively

select hard samples for model learning by gradually increasing the parameter ρ . In this section, we first introduce the increasing strategy of ρ in Sec.5.1. Subsequently, we detail the optimization algorithm for our novel SP²OT algorithm in Sec.5.2, which derives the upper bound of SP²OT and minimizes the upper bound with our newly proposed scaling algorithm alternately. Finally, we provide a summary of the training pipeline in Algorithm 4.

5.1 Increasing strategy of ρ

Selecting high-confidence samples for model learning is crucial in enhancing the quality of learned representations. To achieve that, we adopt a curriculum learning paradigm. Specifically, we select high-confidence samples by total mass constraint ρ and gradually increase the value of ρ . In Eq.(11), instead of starting with 0 and incrementally increasing to 1, we introduce an initial value ρ_0 to mitigate potential issues associated with the model learning from very limited samples in the initial stages. We utilize the sigmoid ramp-up function, a technique commonly employed in semi-supervised learning [67], [68]. Therefore, the increasing strategy of ρ is expressed as follows:

$$\rho = \rho_0 + (1 - \rho_0) \cdot e^{-5(1-t/T)^2}, \quad (14)$$

where T represents the total number of iterations, and t represents the current iteration. We analyze and compare alternate design choices (e.g. linear ramp-up function) in our ablation study. Furthermore, we believe that a more sensible approach to setting ρ involves adaptively increasing it based on the model's learning progress rather than relying on a fixed parameterization tied to the number of iterations. We leave the advanced design of ρ for future work.

5.2 Solver for SP²OT

Solving our SP²OT algorithm directly is challenging due to its inherent complexity. To address this, we employ the Majorization-Minimization optimization algorithm for an efficient solution. Specifically, we leverage the properties of concave functions to linearize the semantic constraint, thereby transforming Eq.(11) into a partial optimal transport problem. Subsequently, we propose a novel method to reformulate this partial optimal transport problem into an unbalanced optimal transport problem, resolving it through the application of the efficient Algorithm 1. These two steps are iteratively performed in an alternating manner until convergence is achieved. This utilization of the Majorization-Minimization optimization strategy enables the effective and efficient resolution of the intricate SP²OT algorithm.

5.2.1 MM algorithm for SP²OT

Unfortunately, with the introduction of semantic regularization, the problem Eq.(11) is not in the same form as Eq.(1), so it can not be solved by simply using the matrix scaling algorithm. To address this problem, we propose utilizing the Majorization-Minimization (MM) algorithm, elaborated in the Appendix 1. This algorithm iteratively minimizes a surrogate function constructed to majorize the original objective function. This iterative approach allows minimizing

Algorithm 2: Semantic regularized pseudo label generation (SP²OT)

Input: Prediction probability matrix \mathbf{P} , adjacency matrix \mathbf{A} ,
 regulation weight $\lambda_1, \lambda_2, \rho, \epsilon$
 $\mathbf{C}_0 \leftarrow -\log \mathbf{P}$
 $\mathbf{Q} \leftarrow \frac{\rho}{N} \mathbf{1}_{N \times K}$
while \mathbf{Q} not converge **do**
 $\mathbf{C} \leftarrow \mathbf{C}_0 - \lambda_1 (\mathbf{A} + \mathbf{A}^\top) \mathbf{Q}$
 $\mathbf{Q} \leftarrow \text{P}^2\text{OT}(\mathbf{C}, \mathbf{Q}, \epsilon, \lambda_2, \rho)$
end
return \mathbf{Q}

the surrogate function instead of the original function at each iteration. For convenience, we first define:

$$f(\mathbf{Q}) = \langle \mathbf{Q}, -\log \mathbf{P} \rangle_F - \lambda_1 \langle \mathbf{A}, \mathbf{Q} \mathbf{Q}^\top \rangle_F.$$

For this function, we have the following proposition:

Proposition 1. $f(\mathbf{Q})$ is a concave function on the feasible set $\mathbb{R}_+^{N \times K}$ if and only if \mathbf{A} is a positive semi-definite matrix on the feasible set $\mathbb{R}_+^{N \times K}$.

The proof is in the Appendix 3. As we adopt the Gaussian kernel function (Eq.(9)), all elements in \mathbf{A} are non-negative. And Π is also non-negative according to the definition in Eq.(12). Consequently, \mathbf{A} is positive semi-definite on Π . Therefore, $f(\mathbf{Q})$ is a concave function on the feasible set Π . Then, at each iteration $t + 1$, given the previously computed \mathbf{Q}_t , we construct a majorized objective function through Taylor expansion:

$$g(\mathbf{Q}|\mathbf{Q}_t) = f(\mathbf{Q}_t) + \langle \nabla f(\mathbf{Q}_t), \mathbf{Q} - \mathbf{Q}_t \rangle_F \quad (15)$$

$$\nabla f(\mathbf{Q}_t) = -\log \mathbf{P} - \lambda_1 (\mathbf{A} + \mathbf{A}^\top) \mathbf{Q}_t. \quad (16)$$

It can be easily verified $f(\mathbf{Q}) \leq g(\mathbf{Q}|\mathbf{Q}_t)$ and $f(\mathbf{Q}_t) = g(\mathbf{Q}_t|\mathbf{Q}_t)$, then $g(\mathbf{Q}|\mathbf{Q}_t)$ is a valid majorized version of $f(\mathbf{Q})$.

Replacing the surrogate function with $f(\mathbf{Q})$ and ignoring the constant term, the updated Eq.(11) is denoted as follows:

$$\min_{\mathbf{Q} \in \Pi} \langle \mathbf{Q}, \nabla f(\mathbf{Q}_t) \rangle_F + \lambda_2 KL(\mathbf{Q}^\top \mathbf{1}_N, \frac{\rho}{K} \mathbf{1}_K) \quad (17)$$

$$\text{s.t. } \Pi = \{ \mathbf{Q} \in \mathbb{R}_+^{N \times K} | \mathbf{Q} \mathbf{1}_K \leq \frac{1}{N} \mathbf{1}_N, \mathbf{1}_N^\top \mathbf{Q} \mathbf{1}_K = \rho \}. \quad (18)$$

The presented problem shares the same form as Eq.(7), and it can be effectively addressed using the efficient scaling algorithm. Consequently, SP²OT can be solved by the MM algorithm, and the detail is presented in Algorithm 2. In the subsequent section, we will provide a comprehensive explanation of the solver for P²OT.

5.2.2 Solver for P²OT

Our approach involves introducing a virtual cluster onto the marginal [69], [70]. This virtual cluster serves the purpose of absorbing the $1 - \rho$ unselected mass, enabling us to transform the total mass constraint into the marginal constraint. Additionally, we replace the KL constraint with a weighted KL constraint to ensure strict adherence to the total mass constraint. As a result, we can reformulate P²OT into a form akin to Eq.(1) and prove their solutions can be interconverted. Subsequently, we resolve this reformulated problem using an efficient scaling algorithm. As shown in Sec.6.3, compared to the generalized scaling solver proposed by [65], our solver is two times faster.

Specifically, we denote the assignment of samples on the virtual cluster as ξ . Then, we extend ξ to \mathbf{Q} , and denote the extended \mathbf{Q} as $\hat{\mathbf{Q}}$ which satisfies the following constraints:

$$\hat{\mathbf{Q}} = [\mathbf{Q}, \xi] \in \mathbb{R}^{N \times (K+1)}, \quad \xi \in \mathbb{R}^{N \times 1}, \quad \hat{\mathbf{Q}} \mathbf{1}_{K+1} = \mathbf{1}_N. \quad (19)$$

Due to $\mathbf{1}_N^\top \mathbf{Q} \mathbf{1}_K = \rho$, we know that,

$$\mathbf{1}_N^\top \hat{\mathbf{Q}} \mathbf{1}_{K+1} = \mathbf{1}_N^\top \mathbf{Q} \mathbf{1}_K + \mathbf{1}_N^\top \xi = 1 \Rightarrow \mathbf{1}_N^\top \xi = 1 - \rho. \quad (20)$$

Therefore,

$$\hat{\mathbf{Q}}^\top \mathbf{1}_N = \begin{bmatrix} \mathbf{Q}^\top \mathbf{1}_N \\ \xi^\top \mathbf{1}_N \end{bmatrix} = \begin{bmatrix} \mathbf{Q}^\top \mathbf{1}_N \\ 1 - \rho \end{bmatrix}. \quad (21)$$

The equation is due to $\mathbf{1}_N^\top \xi = \xi^\top \mathbf{1}_N = 1 - \rho$. We denote $\mathbf{C} = [f(\mathbf{Q}_t), \mathbf{0}_N]$ and replace \mathbf{Q} with $\hat{\mathbf{Q}}$, thus the Eq.(7) can be rewritten as follows:

$$\min_{\hat{\mathbf{Q}} \in \Phi} \langle \hat{\mathbf{Q}}, \mathbf{C} \rangle_F + \lambda KL(\hat{\mathbf{Q}}^\top \mathbf{1}_N, \beta), \quad (22)$$

$$\text{s.t. } \Phi = \{ \hat{\mathbf{Q}} \in \mathbb{R}_+^{N \times (K+1)} | \hat{\mathbf{Q}} \mathbf{1}_{K+1} = \frac{1}{N} \mathbf{1}_N \}, \beta = \begin{bmatrix} \frac{\rho}{K} \mathbf{1}_K \\ 1 - \rho \end{bmatrix}. \quad (23)$$

However, the Eq.(22) is not equivalent to Eq.(17), due to the KL constraint can not guarantee Eq.(21) is strictly satisfied, i.e. $\xi^\top \mathbf{1}_N = 1 - \rho$. To solve this problem, we replace the KL constraint with weighted KL , which enables us to control the constraint strength for each class. The formula of weighted KL is denoted as follows:

$$\hat{K}L(\hat{\mathbf{Q}}^\top \mathbf{1}_N, \beta, \lambda) = \sum_{i=1}^{K+1} \lambda_i [\hat{\mathbf{Q}}^\top \mathbf{1}_N]_i \log \frac{[\hat{\mathbf{Q}}^\top \mathbf{1}_N]_i}{\beta_i}. \quad (24)$$

Therefore, the Eq.(7) can be rewritten as follows:

$$\min_{\hat{\mathbf{Q}} \in \Phi} \langle \hat{\mathbf{Q}}, \mathbf{C} \rangle_F + \hat{K}L(\hat{\mathbf{Q}}^\top \mathbf{1}_N, \beta, \lambda) \quad (25)$$

$$\text{s.t. } \Phi = \{ \hat{\mathbf{Q}} \in \mathbb{R}_+^{N \times (K+1)} | \hat{\mathbf{Q}} \mathbf{1}_{K+1} = \frac{1}{N} \mathbf{1}_N \}, \quad (26)$$

$$\beta = \begin{bmatrix} \frac{\rho}{K} \mathbf{1}_K \\ 1 - \rho \end{bmatrix}, \quad \lambda_{K+1} \rightarrow +\infty. \quad (27)$$

Intuitively, to assure Eq.(21) is strictly satisfied, we set $\lambda_{K+1} \rightarrow +\infty$. This places a substantial penalty on the virtual cluster, compelling the algorithm to assign a size of $1 - \rho$ to the virtual cluster.

Proposition 2. If $\mathbf{C} = [f(\mathbf{Q}_t), \mathbf{0}_N]$, and $\lambda_{:K} = \lambda, \lambda_{K+1} \rightarrow +\infty$, the optimal transport plan $\hat{\mathbf{Q}}^*$ of Eq.(25) can be expressed as:

$$\hat{\mathbf{Q}}^* = [\mathbf{Q}^*, \xi^*], \quad (28)$$

where \mathbf{Q}^* is optimal transport plan of Eq.(17), and ξ^* is the last column of $\hat{\mathbf{Q}}^*$.

The proof is in the Appendix 4. Consequently, we focus on solving Eq.(25) to obtain the optimal $\hat{\mathbf{Q}}^*$.

Proposition 3. Adding a entropy regularization $-\epsilon \mathcal{H}(\hat{\mathbf{Q}})$ to Eq.(25), we can solve it by efficient scaling algorithm. We denote $\mathbf{M} = \exp(-\mathbf{C}/\epsilon)$, $\mathbf{f} = \frac{\lambda}{\lambda + \epsilon}$, $\alpha = \frac{1}{N} \mathbf{1}_N$. The optimal $\hat{\mathbf{Q}}^*$ is denoted as follows:

$$\hat{\mathbf{Q}}^* = \text{diag}(\mathbf{a}) \mathbf{M} \text{diag}(\mathbf{b}), \quad (29)$$

Algorithm 3: Scaling Algorithm for P²OT with stabilization

Input: Cost matrix $-\log \mathbf{P}$, ϵ , λ , ρ , N , K , a large value ι
 $\mathbf{C} \leftarrow [-\log \mathbf{P}, \mathbf{0}_N]$, $\boldsymbol{\lambda} \leftarrow [\lambda, \dots, \lambda, \iota]^\top$
 $\boldsymbol{\beta} \leftarrow [\frac{\rho}{K} \mathbf{1}_K, 1 - \rho]^\top$, $\boldsymbol{\alpha} \leftarrow \frac{1}{N} \mathbf{1}_N$
 $\mathbf{b} \leftarrow \mathbf{1}_{K+1}$, $\mathbf{M} \leftarrow \exp(-\mathbf{C}/\epsilon)$, $\mathbf{f} \leftarrow \frac{\boldsymbol{\lambda}}{\boldsymbol{\lambda} + \epsilon}$
 $\mathbf{u} \leftarrow \mathbf{0}_N$, $\mathbf{v} \leftarrow \mathbf{0}_{K+1}$, $\mathbf{w} \leftarrow \exp(\frac{\mathbf{v}(\mathbf{f}-1)}{\epsilon})$
while \mathbf{b} not converge **do**
 $\mathbf{a} \leftarrow \frac{\boldsymbol{\alpha}}{\mathbf{M}\mathbf{b}}$
 $\mathbf{b} \leftarrow \mathbf{w}(\frac{\boldsymbol{\beta}}{\mathbf{M}^\top \mathbf{a}})^\circ \mathbf{f}$
 if $\max(\max(\mathbf{a}), \max(\mathbf{b}))$ is too large **then**
 $(\mathbf{u}, \mathbf{v}) \leftarrow (\mathbf{u} + \epsilon \log(\mathbf{a}), \mathbf{v} + \epsilon \log(\mathbf{b}))$
 $\mathbf{w} \leftarrow \mathbf{w}\mathbf{f}^{-1}$
 $\mathbf{M} \leftarrow \exp((\mathbf{u} - \mathbf{C} + \mathbf{v})/\epsilon)$
 $(\mathbf{b}, \mathbf{a}) \leftarrow (\mathbf{1}_{K+1}, \mathbf{1}_N)$
 end
end
 $\mathbf{Q} \leftarrow \text{diag}(\mathbf{a})\mathbf{M}\text{diag}(\mathbf{b})$
return $\mathbf{Q}[:, : K]$

where \mathbf{a} , \mathbf{b} are two scaling coefficient vectors and can be derived by the following recursion formula:

$$\mathbf{a} \leftarrow \frac{\boldsymbol{\alpha}}{\mathbf{M}\mathbf{b}}, \quad \mathbf{b} \leftarrow (\frac{\boldsymbol{\beta}}{\mathbf{M}^\top \mathbf{a}})^\circ \mathbf{f}, \quad (30)$$

where \circ denotes Hadamard power, i.e., element-wise power. The recursion will stop until \mathbf{b} converges.

The proof is in the Appendix 5. Moreover, we employ the Log-domain stabilization trick in [65], which absorbs extreme values in \mathbf{a} , \mathbf{b} and keeps them close to 1 to alleviate the numerically imprecise problem and potentially accelerate the convergence. The pseudo-code is shown in Algorithm 3. The efficiency analysis is in the Sec.6.3.

In practical scenarios, solving P²OT for the entire dataset is often impractical. Therefore, we adopt a more feasible approach by implementing mini-batch optimal transport. However, mini-batch OT may face challenges related to insufficient statistical representation due to the limitations imposed by the smaller subset of data. To address this limitation, we introduce a memory buffer that stores a substantial number of sample predictions (e.g., 5120) to ensure the existence of minority clusters. Specifically, before inputting data into P²OT in each iteration, we concatenate predictions from the memory buffer with the current batch predictions to enhance stability while preserving efficiency.

In summary, the details of our training pipeline are outlined in Algorithm 4.

6 EXPERIMENTS

6.1 Experimental Setup

6.1.1 Datasets

To evaluate our method, we have established a realistic and challenging benchmark, including CIFAR100 [11], ImageNet-R (abbreviated as ImgNet-R) [12] and iNaturalist2018 [13] datasets. To quantify the level of class imbalance, we introduce the imbalance ratio denoted as R , calculated as the ratio of N_{max} to N_{min} , where N_{max} represents the largest number of images in a class, and N_{min} represents the smallest. For CIFAR100, as in [40], we artificially construct a long-tailed CIFAR100 dataset with an imbalance ratio of 100. For ImgNet-R, which has renditions of 200 classes resulting in 30k images

Algorithm 4: Overall training strategy

Input: Training dataset \mathcal{D} , initial feature extractor (backbone) f_0 , model f_θ , stochastic transformation T , memory buffer, max_epoch, ρ_0 , λ_1^0 , λ_2 , ϵ , η
 $\mathbf{Z} \leftarrow f_0(\mathcal{D})$
 $\mathbf{A} \leftarrow$ construct k-NNG from \mathbf{Z} by Eq.(9, 10)
for epoch = 1, ..., max_epoch **do**
 for iter = 1, ..., max_iteration **do**
 $\rho \leftarrow \rho_0 + (1 - \rho_0) \cdot e^{-5(1-iter/max_iteration)^2}$
 $\lambda_1 \leftarrow \lambda_1^0 \cdot (1 - \rho)$
 $X, I = \text{Sample}(\mathcal{D})$
 $V_1, V_2 = T(X), T(X)$
 $\mathbf{P}_1, \mathbf{P}_2 = f_\theta(V_1), f_\theta(V_2)$
 // I' is the index of data.
 $\mathbf{M}_1, \mathbf{M}_2, I' = \text{MemoryBuffer}(\mathbf{P}_1, \mathbf{P}_2, I)$
 $\mathbf{A}' = \mathbf{A}[I', I']$
 $\mathbf{Q}_1 = \text{SP}^2\text{OT}(\mathbf{M}_1, \mathbf{A}', \lambda_1, \lambda_2, \rho, \epsilon)$
 $\mathbf{Q}_2 = \text{SP}^2\text{OT}(\mathbf{M}_2, \mathbf{A}', \lambda_1, \lambda_2, \rho, \epsilon)$
 // Swap the prediction of two views.
 $\mathcal{L} \leftarrow \langle \mathbf{Q}_2, -\log \mathbf{P}_1 \rangle_F + \langle \mathbf{Q}_1, -\log \mathbf{P}_2 \rangle_F$
 $\theta \leftarrow \theta - \eta \nabla_\theta \mathcal{L}$
 end
end
return θ

and is inherently imbalanced, we split 20 images per class as the test set, leaving the remaining data as the training set ($R = 13$). Note that the data distribution of ImgNet-R is different from the ImageNet, which is commonly used for training unsupervised pre-trained models, posing a great challenge to its clustering. Consequently, ImgNet-R serves as a valuable resource for assessing the robustness of various methods. Furthermore, we incorporate the iNaturalist2018 dataset, a natural long-tailed dataset frequently used in supervised long-tailed learning [40], [71]. This dataset encompasses 8,142 classes, posing significant challenges for clustering. To mitigate this complexity, we extract subsets of 100, 500, and 1000 classes, creating the iNature100 ($R = 67$), iNature500 ($R = 111$), and iNature1000 ($R = 111$) datasets, respectively. iNature100 is the subset of iNature500, and iNature500 is the subset of iNature1000. The distribution of datasets is in the Appendix 7. We perform evaluations on both the imbalanced training set and the corresponding balanced test set. Note that we do not conduct experiments on ImageNet datasets because the unsupervised pretrained models have trained on the whole balanced ImageNet.

6.1.2 Evaluation Metric

We evaluate our method using the clustering accuracy (ACC) metric averaged over classes, normalized mutual information (NMI), and F1-score. We also provide the adjusted Rand index (ARI) metrics, which is an instance-wise evaluation metric and is not a suitable metric for imbalanced datasets, in the Appendix 9. To provide a more detailed analysis, we rank the classes by size in descending order and divide the dataset into Head, Medium, and Tail categories, maintaining a ratio of 3:4:3 across all datasets. Then, we evaluate performance on the Head, Medium, and Tail, respectively.

6.1.3 Implementation Details

Building upon the advancements in transformer [72] and unsupervised pre-trained models [36], we conduct experiments on the ViT-B16, which is pre-trained with DINO [32]. To provide a comprehensive evaluation, we re-implement a

TABLE 1: Comparison with SOTA methods on different imbalanced training sets. The best results are shown in boldface, and the next best results are indicated with an underscore.

Method	CIFAR100			ImgNet-R			iNature100			iNature500		
	ACC	NMI	F1	ACC	NMI	F1	ACC	NMI	F1	ACC	NMI	F1
DINO	36.6	68.9	31.0	20.5	39.6	22.2	40.1	67.8	34.2	29.8	67.0	24.0
BCL	35.7	66.0	29.9	20.7	40.0	22.4	41.9	67.2	35.4	28.1	64.7	22.4
IIC	27.3 \pm 3.1	65.0 \pm 1.8	23.0 \pm 2.6	18.7 \pm 1.5	39.6 \pm 1.1	15.9 \pm 1.5	28.5 \pm 1.6	63.9 \pm 1.0	22.2 \pm 1.2	13.1 \pm 0.3	58.4 \pm 0.3	7.1 \pm 0.2
PICA	29.8 \pm 0.6	59.9 \pm 0.2	24.0 \pm 0.2	12.6 \pm 0.3	34.0 \pm 0.0	12.1 \pm 0.2	34.8 \pm 2.4	54.8 \pm 0.6	23.8 \pm 1.2	16.3 \pm 0.3	55.9 \pm 0.1	11.3 \pm 0.1
SCAN	37.2 \pm 0.9	69.4 \pm 0.4	31.4 \pm 0.7	21.8 \pm 0.7	42.6 \pm 0.3	21.7 \pm 0.8	38.7 \pm 0.6	66.3 \pm 0.5	28.4 \pm 0.6	29.0 \pm 0.3	66.7 \pm 0.2	21.6 \pm 0.2
SCAN*	30.2 \pm 0.9	68.5 \pm 2.3	25.4 \pm 1.1	23.6 \pm 0.2	44.1 \pm 0.2	22.8 \pm 0.1	39.5 \pm 0.4	68.5 \pm 0.2	30.7 \pm 0.1	19.0 \pm 0.7	65.9 \pm 0.5	12.5 \pm 0.5
CC	29.0 \pm 0.6	60.7 \pm 0.6	24.6 \pm 0.5	12.1 \pm 0.6	30.5 \pm 0.1	11.2 \pm 0.9	28.2 \pm 2.4	56.1 \pm 1.2	20.6 \pm 2.1	16.5 \pm 0.7	55.5 \pm 0.0	12.3 \pm 0.4
DivClust	31.8 \pm 0.3	64.0 \pm 0.4	26.1 \pm 0.8	14.8 \pm 0.2	33.9 \pm 0.4	13.8 \pm 0.2	33.7 \pm 0.2	59.3 \pm 0.5	23.3 \pm 0.7	17.2 \pm 0.5	56.4 \pm 0.3	12.5 \pm 0.4
P ² OT	38.2 \pm 0.8	69.6 \pm 0.3	32.0 \pm 0.9	25.9 \pm 0.9	45.7 \pm 0.5	27.3 \pm 1.4	44.2 \pm 1.2	67.0 \pm 0.6	36.9 \pm 2.0	32.2 \pm 2.0	67.2 \pm 0.3	25.2 \pm 1.7
SP ² OT	39.1 \pm 1.5	67.6 \pm 0.8	32.8 \pm 1.3	27.1 \pm 0.6	<u>44.9</u> \pm 0.7	29.1 \pm 0.6	49.0 \pm 1.3	<u>68.1</u> \pm 0.4	41.8 \pm 0.8	34.1 \pm 0.8	<u>67.2</u> \pm 0.9	27.1 \pm 1.1

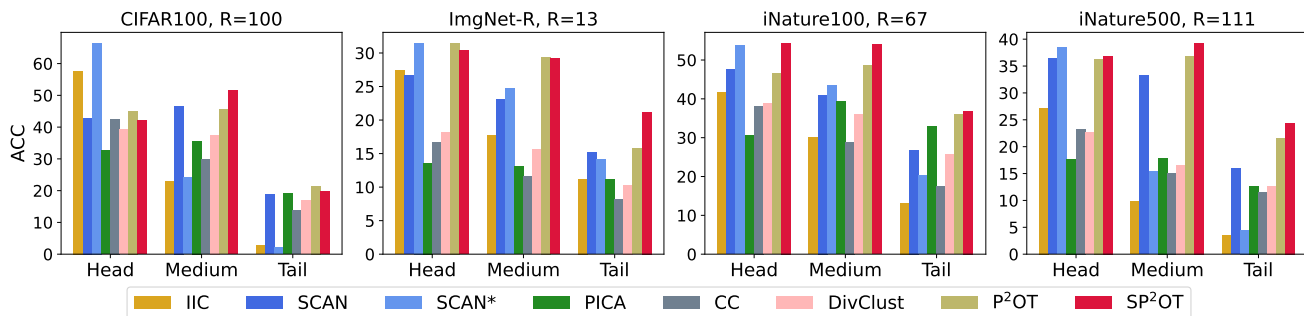


Fig. 1: Head, Medium, and Tail comparison on several datasets.

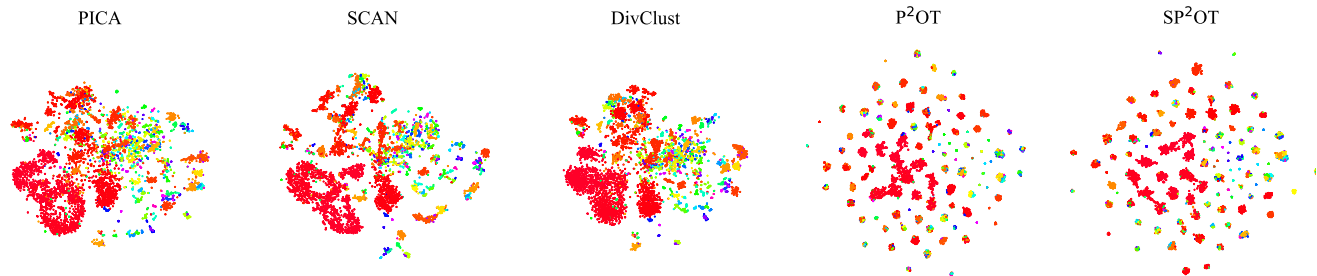


Fig. 2: The T-SNE analysis on iNature100 training set. The primary distinction between them lies in the distribution of the head classes, represented in red (best viewed when zoomed in on screen).

variety of methods from existing literature, encompassing both deep clustering and imbalanced self-supervised learning approaches. Specifically, in the deep clustering domain, we report results for typical methods such as IIC [1], PICA [73], CC [18], SCAN [2], the strong two-stage SCAN* [2] which builds upon SCAN for self-labeling learning, SPICE [7], and the recently proposed DivClust [74]. In the realm of imbalanced self-supervised learning, we implement BCL [6], specifically designed for representation learning with long-tailed data. After representation learning, we proceed to perform clustering in the representation space. Notably, we exclude the re-implementation of [5] as they prune the ResNet, making it challenging to transfer to ViT. It is important to note that all of these methods are trained using the same backbone, data augmentation, and training configurations to ensure a fair comparison. Specifically, we train 50 epochs and adopt the Adam optimizer with

the learning rate decay from $5e-4$ to $5e-6$ for all datasets. The batch size is 512. Further details can be found in the Appendix 8. For hyperparameters, we set λ as 1, ϵ as 0.1, and initial ρ as 0.1. The stop criterion of Alg.3 is when the change of \mathbf{b} is less than $1e-6$, or the iteration reaches 1000. We utilize the loss on training sets for model selection. For evaluation, we conduct experiments with each method three times and report the mean results.

6.2 Main Results

6.2.1 Evaluation on Imbalanced Training Set

In Tab.1, we provide a comprehensive comparison of our method with existing approaches on various imbalanced training sets. On the relatively small-scale CIFAR100 dataset, our SP²OT outperforms the previous state-of-the-art by achieving an increase of 0.9 in ACC, and 0.8 in F1 score. But 2.0% decrease on the NMI metric. On the ImgNet-R datasets,

TABLE 2: Comparison with SOTA methods on different balanced test sets to evaluate generalization ability. The best results are shown in boldface, and the next best results are indicated with an underscore.

Method	CIFAR100			ImgNet-R			iNature100			iNature500		
	ACC	NMI	F1	ACC	NMI	F1	ACC	NMI	F1	ACC	NMI	F1
IIC	29.4 \pm 3.0	56.0 \pm 1.6	21.0 \pm 3.6	21.4 \pm 1.7	53.9 \pm 1.0	17.7 \pm 1.9	35.1 \pm 2.7	75.4 \pm 1.4	25.7 \pm 2.8	19.8 \pm 0.7	73.9 \pm 0.4	10.6 \pm 0.4
PICA	30.3 \pm 0.4	54.5 \pm 0.5	28.3 \pm 0.6	16.6 \pm 0.1	51.8 \pm 0.1	16.6 \pm 0.2	43.6 \pm 3.3	78.2 \pm 1.5	38.7 \pm 3.5	31.4 \pm 0.3	79.6 \pm 0.2	28.3 \pm 0.2
SCAN	37.5 \pm 0.3	<u>63.0</u> \pm 0.1	34.9 \pm 0.4	23.8 \pm 0.8	57.0 \pm 0.4	23.8 \pm 0.9	44.0 \pm 0.9	80.8 \pm 0.5	36.5 \pm 1.1	39.0 \pm 0.1	83.4 \pm 0.1	33.3 \pm 0.3
SCAN*	30.5 \pm 0.6	<u>57.6</u> \pm 2.0	19.8 \pm 0.9	25.3 \pm 0.1	57.1 \pm 0.3	23.5 \pm 0.2	44.8 \pm 0.7	81.9 \pm 0.6	36.8 \pm 1.3	24.3 \pm 0.6	77.0 \pm 0.6	14.4 \pm 0.4
CC	29.1 \pm 1.3	54.2 \pm 0.6	25.6 \pm 1.3	14.7 \pm 0.2	48.5 \pm 0.3	14.1 \pm 0.4	38.2 \pm 1.4	76.3 \pm 0.3	32.4 \pm 0.6	29.7 \pm 1.1	78.3 \pm 0.7	26.5 \pm 1.4
DivClust	31.8 \pm 0.6	58.1 \pm 0.3	28.9 \pm 0.6	16.8 \pm 0.3	50.4 \pm 0.3	16.4 \pm 0.3	42.4 \pm 1.2	78.7 \pm 0.6	36.1 \pm 1.4	31.6 \pm 0.5	79.2 \pm 0.5	27.8 \pm 0.6
P ² OT	38.9 \pm 1.1	63.1 \pm 0.8	35.9 \pm 0.8	27.5 \pm 1.2	58.0 \pm 0.7	28.1 \pm 1.3	50.0 \pm 2.1	83.0 \pm 0.9	44.2 \pm 2.1	42.2 \pm 1.1	84.3 \pm 0.1	37.2 \pm 1.4
SP ² OT	39.0 \pm 1.7	61.8 \pm 1.3	36.6 \pm 1.4	28.3 \pm 0.4	58.1 \pm 0.2	29.9 \pm 0.4	53.8 \pm 0.8	83.8 \pm 0.3	48.1 \pm 1.0	43.6 \pm 0.3	84.7 \pm 0.2	39.0 \pm 0.2

our SP²OT exhibits notable improvements compared to our previous P²OT, with significant increases of 1.2 in accuracy (ACC) and 1.8 in F1 score. This underscores its effectiveness and robustness, particularly in out-of-distribution scenarios. While our method achieves superior clustering performance, as evidenced by higher ACC or F1 scores, it also leads to a relatively uniform distribution, which increases the denominator of the NMI metric and results in a decrease in the NMI metric. A detailed explanation can be found in the Appendix 10.

When applied to the fine-grained iNature datasets, our approach consistently delivers substantial performance gains across each subset in terms of ACC and F1 scores. Specifically, on ACC, we achieve improvements of 4.8 on iNature100 and 1.9 on iNature500. On the F1 score, we obtain improvements of 4.9 and 1.9 on the two datasets, respectively. In terms of NMI, compared to P²OT, we observe a 1.1 improvement on iNature100, but compared to SCAN*, there is still a decrease of 0.4. It’s worth noting that our method is an efficient one-stage approach, in contrast to SCAN*, which is a two-stage pseudo-labeling-based method. Additionally, another pseudo-labeling-based method, SPICE, exhibits a degenerate solution in the imbalance scenario (see Appendix 8). These results indicate that naive pseudo-labeling methods encounter significant challenges, emphasizing our method’s superiority in handling imbalance scenarios.

In addition, we provide a detailed analysis of the results for the Head, Medium, and Tail classes, offering a more comprehensive understanding of our method’s performance across different class sizes. As depicted in Fig. 1, our improvements are predominantly driven by the Medium and Tail classes, especially in challenging scenarios like ImgNet-R and iNature500, although our results show some reductions in performance for the Head classes. These results highlight the effectiveness of our SP²OT algorithm in generating imbalance-aware pseudo-labels, making it particularly advantageous for the Medium and Tail classes.

Furthermore, in Fig. 2, we present a T-SNE [75] comparison of features before the clustering head. The T-SNE results illustrate that our method learns more distinct clusters, particularly benefiting Medium and Tail classes. In particular, in comparison to P²OT, the head cluster in SP²OT (depicted in red) is more separable.

6.2.2 Evaluation on Balanced Test Set

To assess the generalization ability of our method in an inductive setting, we conducted experiments on the balanced

TABLE 3: Comparison with SOTA methods on iNature1000. The best results are shown in boldface, and the next best results are indicated with an underscore.

Method	Train			Test		
	ACC	NMI	F1	ACC	NMI	F1
IIC	7.8 \pm 0.5	56.9 \pm 0.4	4.2 \pm 0.2	13.3 \pm 1.0	71.2 \pm 0.6	5.1 \pm 0.7
PICA	12.4 \pm 0.2	55.0 \pm 0.1	8.5 \pm 0.1	28.3 \pm 0.2	80.0 \pm 0.2	26.0 \pm 0.1
SCAN	26.2 \pm 0.2	<u>68.0</u> \pm 0.0	19.6 \pm 0.1	36.5 \pm 0.3	84.2 \pm 0.1	31.7 \pm 0.4
SCAN*	10.5 \pm 0.2	63.9 \pm 0.5	6.4 \pm 0.2	14.5 \pm 0.2	72.8 \pm 0.3	5.8 \pm 0.2
CC	12.1 \pm 0.4	55.2 \pm 0.4	9.1 \pm 0.4	26.6 \pm 0.5	78.7 \pm 0.2	24.0 \pm 0.8
DivClust	13.0 \pm 0.2	56.0 \pm 0.3	9.5 \pm 0.2	26.9 \pm 0.1	78.8 \pm 0.3	24.3 \pm 0.2
P ² OT	26.7 \pm 0.5	67.4 \pm 0.4	19.9 \pm 0.4	37.7 \pm 0.2	84.4 \pm 0.2	33.0 \pm 0.2
SP ² OT	28.0 \pm 0.8	68.6 \pm 0.1	21.6 \pm 0.9	38.9 \pm 1.0	84.8 \pm 0.3	34.0 \pm 1.0

test sets of the three datasets. We did not compare with DINO and BCL on the test sets because they are not designed for transductive settings. As shown in Table 2, on CIFAR100, our method slightly outperforms P²OT in terms of ACC and F1 score, with a decrease (1.3) in NMI. This decrease in NMI may be attributed to the fact that SP²OT results in a more uniform distribution than P²OT on CIFAR100. Notably, SP²OT outperforms the state-of-the-art P²OT on ImgNet-R, iNature100, and iNature500 by a significant margin, demonstrating its robustness in out-of-distribution scenarios and fine-grained scenarios.

6.2.3 Evaluation on Large-scale iNature1000

To further evaluate the scalability of our method, we conducted experiments on the large-scale iNature1000 dataset, which poses a significant challenge. As shown in Table 3, our method achieves the best performance on both training and test sets across all metrics. Specifically, our method outperforms the previous state-of-the-art method, P²OT, by 1.3 in ACC, 1.2 in NMI, and 1.7 in F1 score on the training set. On the test set, our method achieves improvements of 1.2, 0.4, and 1.0 in ACC, NMI, and F1 scores, respectively. These results underscore the scalability of our method in large-scale scenarios.

6.3 Ablation Study

6.3.1 Component Analysis

To assess the KL constraint, the progressive ρ , and the semantic regularization, we conduct ablation experiments to analyze their individual contributions. As shown in Table 4, we compare our full SP²OT method with three ablated versions: OT, POT, UOT, and P²OT. OT [25] imposes equality

TABLE 4: Analysis of different formulations. SLA is proposed by [51] in semi-supervised learning. OT [25], POT, UOT, and P²OT are variants of our SP²OT. P²OT removes the semantic relation regularization in SP²OT. POT substitutes the *KL* constraint in P²OT with the equality constraint. UOT removes the progressive ρ in P²OT.

Formulation	CIFAR100				ImgNet-R				iNature500			
	Head	Medium	Tail	ACC	Head	Medium	Tail	ACC	Head	Medium	Tail	ACC
SLA	-	-	-	3.26	-	-	-	1.00	-	-	-	6.33
OT	35.0	30.2	18.7	28.2	24.4	19.3	10.7	18.2	27.1	27.5	16.4	24.1
POT	39.6	42.9	14.5	33.4	25.5	23.3	17.6	22.2	31.7	32.7	19.7	28.5
UOT	43.4	42.5	19.6	35.9	27.7	23.9	14.6	22.2	32.2	29.0	18.3	26.7
P ² OT	45.1	45.5	21.6	38.2	31.5	29.3	16.1	25.9	36.3	37.0	21.6	32.2
SP ² OT	42.0	51.6	19.8	39.1	30.4	29.2	21.2	27.1	36.9	39.3	24.4	34.1

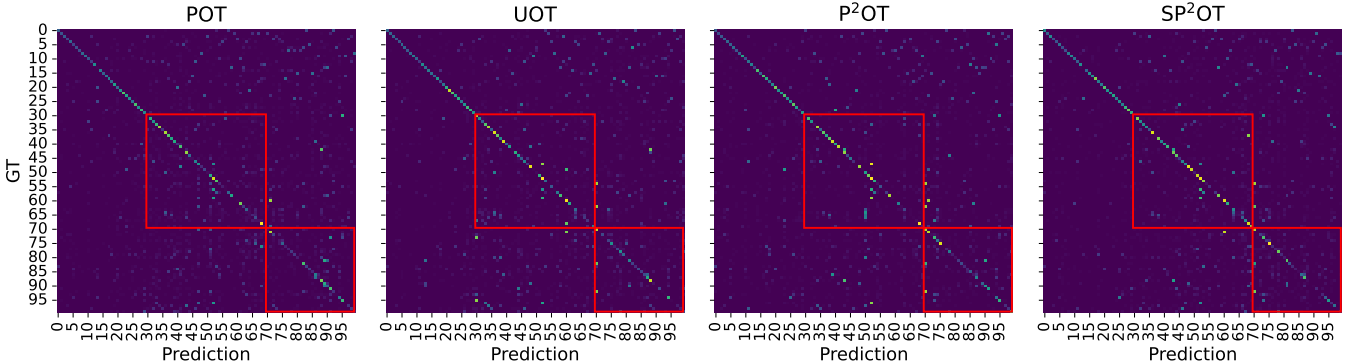


Fig. 3: Confusion matrix on the balanced CIFAR100 test set. The two red rectangles represent the Medium and Tail classes.

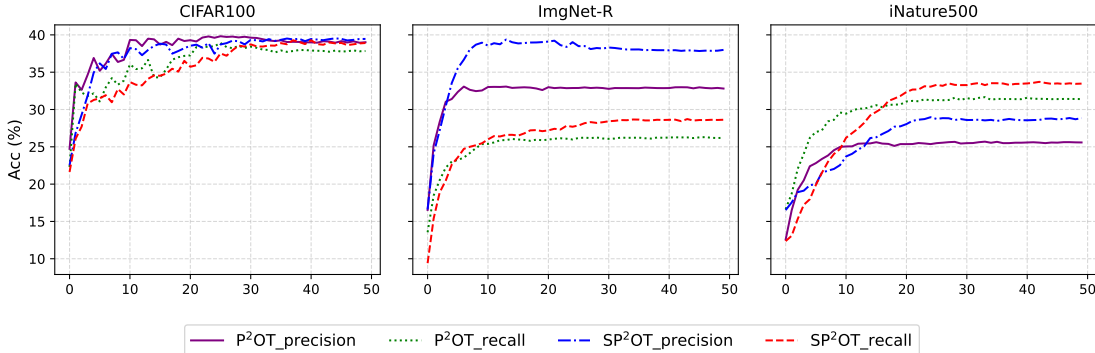


Fig. 4: Precision, Recall analysis of P²OT and SP²OT on train dataset with different training epoch.

constraint on cluster size and without the progressive ρ component. POT signifies the replacement of the *KL* term in the P²OT formulation with a typical uniform constraint. UOT denotes the removal of the progressive ρ component from the P²OT formulation. And P²OT denotes SP²OT to remove the semantic regularization. Furthermore, we also compare with SLA [51], which relaxes the equality constraint of POT by utilizing an upper bound. However, due to this relaxation, samples are erroneously assigned to a single cluster in the early stages, rendering its failure for clustering imbalanced data. We detail their formulation and further analysis in Appendix 12. The results show POT and UOT both significantly surpass the OT, indicating that the *KL* constraint and the progressive ρ components yield satisfactory effects. Compared to POT, P²OT achieves improvements of 5.8, 3.8, and 3.6 on CIFAR100, ImgNet-R, and iNature500, respectively. The improvement is mainly from Head and Tail classes, demonstrating that P²OT with *KL* constraint can generate imbalanced pseudo labels. Compared to UOT, P²OT

realizes gains of 2.3, 3.8, and 5.4 on CIFAR100, ImgNet-R, and iNature500, respectively. SP²OT, which equips P²OT with a novel semantic relation regularization, further improves P²OT by a sizeable margin, and the improvements are mainly from Medium or Tail classes.

Additionally, as depicted in Fig.3, SP²OT exhibits better results on medium classes, whereas P²OT demonstrates better results on head classes. Furthermore, we analyze precision and recall metrics for both the P²OT and SP²OT algorithms. As shown in Fig.4, SP²OT exhibits a gradual increase in precision and recall, comparable to or slightly slower than P²OT in the initial stages. However, SP²OT outperforms P²OT, achieving higher results in the end. We posit that the introduction of semantic constraints imposes an additional constraint on the learning process, leading to a more gradual improvement. This effect helps prevent the model from quickly fitting to noise, ultimately contributing to the superior performance of SP²OT in later stages.

TABLE 5: Analysis of ρ_0 and different ramp up function. Fixed denotes ρ as a constant value.

ρ_0	Sigmoid					Linear			Fixed	
	0.00	0.05	0.1	0.15	0.2	0	0.1	0.2	0.1	0.2
CIFAR100	32.9	37.9	38.2	36.3	37.6	35.0	36.6	36.8	37.4	37.1
ImgNet-R	26.5	27.2	25.9	26.0	26.6	25.8	28.5	23.0	25.5	24.7
iNature500	32.6	31.7	32.2	32.8	32.9	31.9	32.0	30.5	29.9	30.3

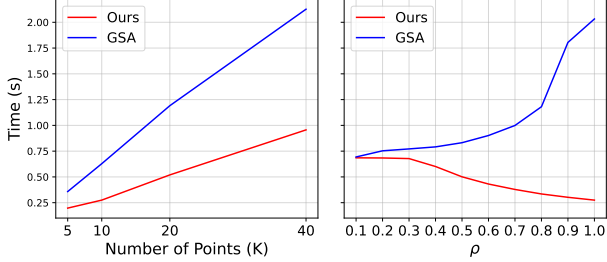


Fig. 5: Time cost comparison of our solver with Generalized Scaling Algorithm (GSA).

6.3.2 Pseudo Label Quality Analysis

To provide a deeper understanding, we conduct an analysis of the pseudo-label quality generated by our P²OT. We evaluate precision and recall metrics to assess the pseudo-label quality for the entire training set. Notably, our P²OT algorithm conducts selection through reweighting, rather than hard selection. Consequently, we reweight each sample and present the weighted precision and recall results. As depicted in Fig.6, our weighted precision and recall consistently outperform precision and recall across different epochs. In the early stages, weighted precision and recall exhibit more rapid improvements compared to precision and recall, demonstrating the effectiveness of our selection strategy. However, they eventually plateau around 10 epochs ($\rho \approx 0.15$), converging gradually with precision and recall. The decline observed in weighted precision and recall over time suggests that our current ramp-up function may not be optimal, and raising to 1 for ρ may not be necessary. We believe that the ramp-up strategy for ρ should be adaptive to the model’s learning progress. In this paper, we have adopted a typical sigmoid ramp-up strategy, and leave more advanced designs for future work.

6.3.3 Efficiency Analysis

To demonstrate the efficiency of our solver, we perform a comparison between our solver and the Generalized Scaling Algorithm (GSA) proposed by [65] for P²OT. The pseudocode of GSA is in the Appendix 13. This comparison is conducted on iNautre1000 using identical conditions (NVIDIA TITAN RTX, $\epsilon = 0.1$, $\lambda = 1$), without employing any acceleration strategies for both. To ensure the comprehensiveness of our time cost analysis, we conduct experiments by varying both the number of data points and the ρ value. Subsequently, we average the time costs for different numbers of data points across different ρ values and vice versa. The results presented in Fig.5 reveal several insights: 1) the time cost of both methods increases near linearly with the number of points; 2) as ρ approaches 1, the time cost of GSA increases rapidly due to the tightening inequality constraint, whereas our time cost decreases; 3) as shown in the left figure, our

solver is $2\times$ faster than GSA. Those results demonstrate the efficiency of our solver proposed in Sec.5.2.2.

6.3.4 Analysis of ρ

The choice of initial ρ_0 and the specific ramp-up strategy are important hyperparameters. Therefore, in this section, we systematically investigate the impact of varying ρ_0 values and alternative ramp-up strategy on P²OT, which removes the semantic regularization of SP²OT and is more efficiency to train. The term "Linear" signifies that ρ is increased to 1 from ρ_0 using a linear function, while "Fixed" indicates that ρ remains constant as ρ_0 . The results in Table 5 provide several important insights: 1) Our method exhibits consistent performance across various ρ_0 values when using the sigmoid ramp-up function, highlighting its robustness on datasets like ImgNet-R and iNature500; 2) The linear ramp-up strategy, although slightly less effective than sigmoid, still demonstrates the importance of gradually increasing ρ during the early training stage; 3) The fixed ρ approach results in suboptimal performance, underscoring the necessity of having a dynamically increasing ρ . These findings suggest that a good starting value for ρ_0 is around 0.1, and it should be progressively increased during training.

6.3.5 Analysis of λ_1 and k for semantic regularization

In our SP²OT algorithm, the λ_1 affects the semantic regulation strength. As shown in Table 6, "500", "1000", "2000" is the value of λ_1^0 , which is the initial value of λ_1 and decays with the training process as in Eq.13. "Fix" donates λ_1 is fixed to 1000 during the training process. We conduct these experiments with $k=20$. we observed that a larger λ_1 is preferred for CIFAR100 and iNature500, while a smaller one is preferred for ImgNet-R. We suggest to set λ_1 as 1000, which achieves satisfactory results on all datasets.

Additionally, we can observe that when λ_1 is fixed at 1000, the performance of the model on CIFAR100 and ImgNet-R shows little improvement, while there is a sizeable decline on iNature500. This is because the k-NNG constructed on these two datasets is clean and reliable. In contrast, iNature500 has a larger number of categories, resulting in more noise within the k-NNG. Therefore, not applying weight decay would constrain the model’s learning in this scenario, showing the necessity of semantic regularization decline.

The parameter k is the number of nearest neighbors selected in the dataset for each sample in k-NNG. We conduct experiments with $k=10, 20, 50$ as shown in Table 7. In these experiments, we set $\lambda_1^0=1000$. Empirically, with a small k , the semantic regularization is too weak to guide the pseudo-label generation, while with a large k , the semantic regularization will introduce large noise from the initial feature space and hurt the performance. From the results, we can see that $k=20$ is a suitable choice for all three datasets and is the default setting in our experiments.

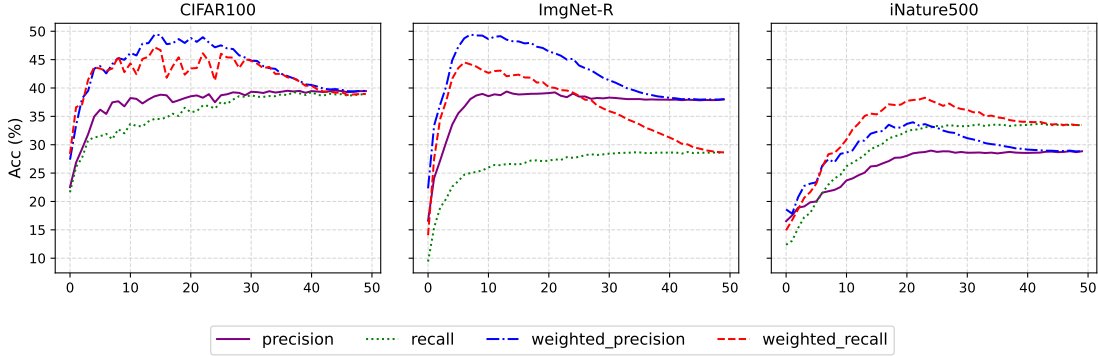


Fig. 6: Precision, Recall analysis on train dataset with different training epoch. The weighted precision and recall are derived by reweighting each sample by our SP²OT algorithm.

TABLE 6: Analysis of λ_1 on different datasets.

λ_1	500	1000	2000	Fix(1000)
CIFAR100	36.0	39.1	37.8	39.4
ImgNet-R	28.7	27.1	27.2	27.8
iNature500	31.9	34.1	34.0	32.3

TABLE 7: Analysis of k for k-NNG on different datasets.

k	10	20	50
CIFAR100	38.6	39.1	38.4
ImgNet-R	28.8	27.1	28.8
iNature500	32.2	34.1	32.6

TABLE 8: Analysis of the kernel function.

$K(\cdot, \cdot)$	gaussian	cosine
CIFAR100	39.1	37.9
ImgNet-R	27.1	28.3
iNature500	34.1	33.5

6.3.6 Analysis of the kernel function

In our method, we use the Gaussian kernel, which is non-negative and ensures the construction of the adjacency matrix is positive semi-definite in Eq.(10). To validate the effect of the different kernel functions, we further conduct experiments with the Cosine kernel, which is:

$$K_{cos}(z_i, z_j) = \frac{z_i \cdot z_j}{\|z_i\| \|z_j\|} \tag{31}$$

While it doesn't offer a theoretical guarantee for the positive semi-definite property of the adjacency matrix, given the presence of negative values, we consistently observe that the constructed adjacency matrix tends to be positive semi-definite in practical scenarios. The corresponding results are detailed in Table 8. In our experiments, we set $\lambda_1^0 = 1000$ and $k = 20$. It is noteworthy that the Gaussian kernel outperforms the Cosine kernel on CIFAR100 and iNature500, while the Cosine kernel exhibits slightly better performance on ImgNet-R. These findings underscore the general applicability of our method across different kernels, showcasing its versatility and effectiveness in diverse experimental settings.

6.4 Limitation

While our method demonstrates effective improvements, there are several avenues for exploration in future research. Firstly, our MM-based solver for SP²OT requires iteration to optimize, necessitating a more efficient algorithm. Secondly, the curriculum strategy employed in our method follows a predetermined incremental approach, which is a suboptimal solution; therefore, a more adaptive strategy is warranted.

7 CONCLUSIONS

In this paper, we introduce a more practical problem known as "deep imbalanced clustering", which is designed to learn representations and semantic clusters from unlabeled imbalanced data, aiming to bridge the gap between practical scenarios and existing research. In response to this challenging problem, we present a novel progressive pseudo-label (PL)-based learning framework. This framework formulates the pseudo-label generation as a semantic regularized progressive partial optimal transport (SP²OT) algorithm. The SP²OT algorithm is instrumental in generating high-quality pseudo-labels by concurrently considering imbalanced cluster distribution, high-confidence sample selection, and semantic relations. This comprehensive approach significantly enhances model learning and clustering performance, offering a promising solution to the complexities inherent in deep imbalanced clustering scenarios.

To address the novel SP²OT algorithm, we utilize the MM algorithm. Initially, leveraging the properties of concave functions, we derive an upper bound for SP²OT through Taylor expansion. The resulting upper bound of SP²OT takes the form of a Progressive Partial Optimal Transport (P²OT) problem. To enhance the efficiency of solving P²OT, we introduce a virtual cluster and incorporate a weighted KL constraint. Subsequently, by imposing specific constraints, we transform P²OT into an unbalanced optimal transport problem, amenable to an efficient solution through a scaling algorithm. Consequently, the SP²OT is approximately solved through an iterative process that alternates between these two steps. To demonstrate the effectiveness of our approach, we establish a new benchmark comprising a human-curated long-tailed CIFAR100 dataset, challenging ImageNet-R datasets, and several large-scale fine-grained iNature datasets. Through extensive experiments on these datasets, we validate the superiority of our proposed method.

REFERENCES

- [1] X. Ji, J. F. Henriques, and A. Vedaldi, "Invariant information clustering for unsupervised image classification and segmentation," in *Proceedings of the IEEE/CVF International Conference on Computer Vision*, 2019, pp. 9865–9874.
- [2] W. Van Gansbeke, S. Vandenhende, S. Georgoulis, M. Proesmans, and L. Van Gool, "Scan: Learning to classify images without labels," in *Proceedings of the European Conference on Computer Vision*, 2020.
- [3] M. Ronen, S. E. Finder, and O. Freifeld, "Deepdpm: Deep clustering with an unknown number of clusters," in *Conference on Computer Vision and Pattern Recognition*, 2022.
- [4] Z. Dang, C. Deng, X. Yang, K. Wei, and H. Huang, "Nearest neighbor matching for deep clustering," in *Proceedings of the IEEE/CVF Conference on Computer Vision and Pattern Recognition (CVPR)*, June 2021, pp. 13 693–13 702.
- [5] Z. Jiang, T. Chen, B. J. Mortazavi, and Z. Wang, "Self-damaging contrastive learning," in *International Conference on Machine Learning*. PMLR, 2021, pp. 4927–4939.
- [6] Z. Zhou, J. Yao, Y.-F. Wang, B. Han, and Y. Zhang, "Contrastive learning with boosted memorization," in *International Conference on Machine Learning*. PMLR, 2022, pp. 27 367–27 377.
- [7] C. Niu, H. Shan, and G. Wang, "Spice: Semantic pseudo-labeling for image clustering," *IEEE Transactions on Image Processing*, vol. 31, pp. 7264–7278, 2022.
- [8] E. Arazo, D. Ortego, P. Albert, N. E. O'Connor, and K. McGuinness, "Pseudo-labeling and confirmation bias in deep semi-supervised learning," in *2020 International Joint Conference on Neural Networks (IJCNN)*. IEEE, 2020, pp. 1–8.
- [9] B. Kang, S. Xie, M. Rohrbach, Z. Yan, A. Gordo, J. Feng, and Y. Kalantidis, "Decoupling representation and classifier for long-tailed recognition," in *Eighth International Conference on Learning Representations (ICLR)*, 2020.
- [10] C. Zhang, H. Ren, and X. He, "P²ot: Progressive partial optimal transport for deep imbalanced clustering," 2024.
- [11] A. Krizhevsky, G. Hinton *et al.*, "Learning multiple layers of features from tiny images," 2009.
- [12] D. Hendrycks, S. Basart, N. Mu, S. Kadavath, F. Wang, E. Dorundo, R. Desai, T. Zhu, S. Parajuli, M. Guo, D. Song, J. Steinhardt, and J. Gilmer, "The many faces of robustness: A critical analysis of out-of-distribution generalization," *ICCV*, 2021.
- [13] G. Van Horn, O. Mac Aodha, Y. Song, Y. Cui, C. Sun, A. Shepard, H. Adam, P. Perona, and S. Belongie, "The inaturalist species classification and detection dataset," in *Proceedings of the IEEE conference on computer vision and pattern recognition*, 2018, pp. 8769–8778.
- [14] S. Zhou, H. Xu, Z. Zheng, J. Chen, J. Bu, J. Wu, X. Wang, W. Zhu, M. Ester *et al.*, "A comprehensive survey on deep clustering: Taxonomy, challenges, and future directions," *arXiv preprint arXiv:2206.07579*, 2022.
- [15] Z. Huang, J. Chen, J. Zhang, and H. Shan, "Learning representation for clustering via prototype scattering and positive sampling," *IEEE Transactions on Pattern Analysis and Machine Intelligence*, 2022.
- [16] J. Chang, L. Wang, G. Meng, S. Xiang, and C. Pan, "Deep adaptive image clustering," in *Proceedings of the IEEE international conference on computer vision*, 2017, pp. 5879–5887.
- [17] Y. Tao, K. Takagi, and K. Nakata, "Clustering-friendly representation learning via instance discrimination and feature decorrelation," in *International Conference on Learning Representations*, 2020.
- [18] Y. Li, P. Hu, Z. Liu, D. Peng, J. T. Zhou, and X. Peng, "Contrastive clustering," in *Proceedings of the AAAI Conference on Artificial Intelligence*, vol. 35, no. 10, 2021, pp. 8547–8555.
- [19] Y. Shen, Z. Shen, M. Wang, J. Qin, P. Torr, and L. Shao, "You never cluster alone," *Advances in Neural Information Processing Systems*, vol. 34, pp. 27 734–27 746, 2021.
- [20] I. Ben-Shaul, R. Shwartz-Ziv, T. Galanti, S. Dekel, and Y. LeCun, "Reverse engineering self-supervised learning," *arXiv preprint arXiv:2305.15614*, 2023.
- [21] D.-H. Lee *et al.*, "Pseudo-label: The simple and efficient semi-supervised learning method for deep neural networks," in *Workshop on challenges in representation learning, ICML*, vol. 3, no. 2. Atlanta, 2013, p. 896.
- [22] K. Sohn, D. Berthelot, N. Carlini, Z. Zhang, H. Zhang, C. A. Raffel, E. D. Cubuk, A. Kurakin, and C.-L. Li, "Fixmatch: Simplifying semi-supervised learning with consistency and confidence," *Advances in Neural Information Processing Systems*, vol. 33, pp. 596–608, 2020.
- [23] B. Zhang, Y. Wang, W. Hou, H. Wu, J. Wang, M. Okumura, and T. Shinozaki, "Flexmatch: Boosting semi-supervised learning with curriculum pseudo labeling," *Advances in Neural Information Processing Systems*, vol. 34, pp. 18 408–18 419, 2021.
- [24] M. Caron, P. Bojanowski, A. Joulin, and M. Douze, "Deep clustering for unsupervised learning of visual features," in *Proceedings of the European conference on computer vision (ECCV)*, 2018, pp. 132–149.
- [25] Y. M. Asano, C. Rupprecht, and A. Vedaldi, "Self-labelling via simultaneous clustering and representation learning," in *International Conference on Learning Representations (ICLR)*, 2020.
- [26] Y. Bengio, A. Courville, and P. Vincent, "Representation learning: A review and new perspectives," *IEEE transactions on pattern analysis and machine intelligence*, vol. 35, no. 8, pp. 1798–1828, 2013.
- [27] L. Jing and Y. Tian, "Self-supervised visual feature learning with deep neural networks: A survey," *IEEE transactions on pattern analysis and machine intelligence*, vol. 43, no. 11, pp. 4037–4058, 2020.
- [28] T. Chen, S. Kornblith, M. Norouzi, and G. Hinton, "A simple framework for contrastive learning of visual representations," in *International conference on machine learning*. PMLR, 2020, pp. 1597–1607.
- [29] K. He, H. Fan, Y. Wu, S. Xie, and R. Girshick, "Momentum contrast for unsupervised visual representation learning," in *Proceedings of the IEEE/CVF conference on computer vision and pattern recognition*, 2020, pp. 9729–9738.
- [30] X. Wang and G.-J. Qi, "Contrastive learning with stronger augmentations," *IEEE transactions on pattern analysis and machine intelligence*, vol. 45, no. 5, pp. 5549–5560, 2022.
- [31] H. Xu, X. Zhang, H. Li, L. Xie, W. Dai, H. Xiong, and Q. Tian, "Seed the views: Hierarchical semantic alignment for contrastive representation learning," *IEEE Transactions on Pattern Analysis and Machine Intelligence*, vol. 45, no. 3, pp. 3753–3767, 2022.
- [32] M. Caron, H. Touvron, I. Misra, H. Jégou, J. Mairal, P. Bojanowski, and A. Joulin, "Emerging properties in self-supervised vision transformers," in *Proceedings of the IEEE/CVF international conference on computer vision*, 2021, pp. 9650–9660.
- [33] X. Chen and K. He, "Exploring simple siamese representation learning," in *Proceedings of the IEEE/CVF conference on computer vision and pattern recognition*, 2021, pp. 15 750–15 758.
- [34] J.-B. Grill, F. Strub, F. Altché, C. Tallec, P. Richemond, E. Buchatskaya, C. Doersch, B. Avila Pires, Z. Guo, M. Gheshlaghi Azar *et al.*, "Bootstrap your own latent—a new approach to self-supervised learning," *Advances in neural information processing systems*, vol. 33, pp. 21 271–21 284, 2020.
- [35] Z. Huang, X. Jin, C. Lu, Q. Hou, M.-M. Cheng, D. Fu, X. Shen, and J. Feng, "Contrastive masked autoencoders are stronger vision learners," *IEEE Transactions on Pattern Analysis and Machine Intelligence*, 2023.
- [36] K. He, X. Chen, S. Xie, Y. Li, P. Dollár, and R. Girshick, "Masked autoencoders are scalable vision learners," in *Proceedings of the IEEE/CVF conference on computer vision and pattern recognition*, 2022, pp. 16 000–16 009.
- [37] I. Radosavovic, T. Xiao, S. James, P. Abbeel, J. Malik, and T. Darrell, "Real-world robot learning with masked visual pre-training," in *Conference on Robot Learning*. PMLR, 2023, pp. 416–426.
- [38] R. Balestriero, M. Ibrahim, V. Sobal, A. Morcos, S. Shekhar, T. Goldstein, F. Bordes, A. Bardes, G. Mialon, Y. Tian *et al.*, "A cookbook of self-supervised learning," *arXiv preprint arXiv:2304.12210*, 2023.
- [39] H. Liu, J. Z. HaoChen, A. Gaidon, and T. Ma, "Self-supervised learning is more robust to dataset imbalance," 2022.
- [40] K. Cao, C. Wei, A. Gaidon, N. Arechiga, and T. Ma, "Learning imbalanced datasets with label-distribution-aware margin loss," in *Advances in Neural Information Processing Systems*, 2019.
- [41] S. Zhang, Z. Li, S. Yan, X. He, and J. Sun, "Distribution alignment: A unified framework for long-tail visual recognition," in *Proceedings of the IEEE/CVF Conference on Computer Vision and Pattern Recognition (CVPR)*, June 2021, pp. 2361–2370.
- [42] A. K. Menon, S. Jayasumana, A. S. Rawat, H. Jain, A. Veit, and S. Kumar, "Long-tail learning via logit adjustment," *arXiv preprint arXiv:2007.07314*, 2020.
- [43] Y. Zhang, B. Kang, B. Hooi, S. Yan, and J. Feng, "Deep long-tailed learning: A survey," *IEEE Transactions on Pattern Analysis and Machine Intelligence*, 2023.
- [44] C. Villani *et al.*, *Optimal transport: old and new*. Springer, 2009, vol. 338.

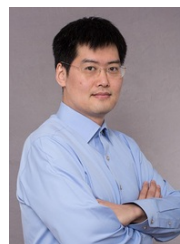
- [45] G. Peyré, M. Cuturi *et al.*, “Computational optimal transport,” *Center for Research in Economics and Statistics Working Papers*, no. 2017-86, 2017.
- [46] A. Khamis, R. Tsuchida, M. Tarek, V. Rolland, and L. Petersson, “Earth movers in the big data era: A review of optimal transport in machine learning,” *arXiv preprint arXiv:2305.05080*, 2023.
- [47] N. Lahn, S. Raghvendra, and K. Zhang, “A combinatorial algorithm for approximating the optimal transport in the parallel and mpc settings,” *Advances in Neural Information Processing Systems*, vol. 36, 2024.
- [48] A. Phatak, S. Raghvendra, C. Tripathy, and K. Zhang, “Computing all optimal partial transports,” in *The Eleventh International Conference on Learning Representations*, 2022.
- [49] C. Frogner, C. Zhang, H. Mobahi, M. Araya, and T. A. Poggio, “Learning with a wasserstein loss,” *Advances in neural information processing systems*, vol. 28, 2015.
- [50] I. Gulrajani, F. Ahmed, M. Arjovsky, V. Dumoulin, and A. C. Courville, “Improved training of wasserstein gans,” *Advances in neural information processing systems*, vol. 30, 2017.
- [51] K. S. Tai, P. D. Bailis, and G. Valiant, “Sinkhorn label allocation: Semi-supervised classification via annealed self-training,” in *International Conference on Machine Learning*. PMLR, 2021, pp. 10 065–10 075.
- [52] F. Taherkhani, A. Dabouei, S. Soleymani, J. Dawson, and N. M. Nasrabadi, “Transporting labels via hierarchical optimal transport for semi-supervised learning,” in *Computer Vision—ECCV 2020: 16th European Conference, Glasgow, UK, August 23–28, 2020, Proceedings, Part IV 16*. Springer, 2020, pp. 509–526.
- [53] M. Caron, I. Misra, J. Mairal, P. Goyal, P. Bojanowski, and A. Joulin, “Unsupervised learning of visual features by contrasting cluster assignments,” *Advances in Neural Information Processing Systems*, vol. 33, pp. 9912–9924, 2020.
- [54] R. Flamary, N. Courty, D. Tuia, and A. Rakotomamonjy, “Optimal transport for domain adaptation,” *IEEE Trans. Pattern Anal. Mach. Intell.*, vol. 1, pp. 1–40, 2016.
- [55] W. Chang, Y. Shi, H. Tuan, and J. Wang, “Unified optimal transport framework for universal domain adaptation,” *Advances in Neural Information Processing Systems*, vol. 35, pp. 29 512–29 524, 2022.
- [56] Y. Liu, Z. Zhou, and B. Sun, “Cot: Unsupervised domain adaptation with clustering and optimal transport,” in *Proceedings of the IEEE/CVF Conference on Computer Vision and Pattern Recognition (CVPR)*, June 2023, pp. 19 998–20 007.
- [57] W. Chang, Y. Shi, and J. Wang, “Csot: Curriculum and structure-aware optimal transport for learning with noisy labels,” in *Thirty-seventh Conference on Neural Information Processing Systems*, 2023.
- [58] W. Wang, F. Wen, Z. Yan, and P. Liu, “Optimal transport for unsupervised denoising learning,” *IEEE Transactions on Pattern Analysis and Machine Intelligence*, vol. 45, no. 2, pp. 2104–2118, 2022.
- [59] D. Luo, H. Xu, and L. Carin, “Differentiable hierarchical optimal transport for robust multi-view learning,” *IEEE Transactions on Pattern Analysis and Machine Intelligence*, 2022.
- [60] C. Zhang, R. Xu, and X. He, “Novel class discovery for long-tailed recognition,” *Transactions on Machine Learning Research*, 2023.
- [61] L. Kantorovich, “On the transfer of masses (in russian),” *Doklady Akademii Nauk*, vol. 37, pp. 227–229, 1942.
- [62] M. Liero, A. Mielke, and G. Savaré, “Optimal entropy-transport problems and a new hellinger–kantorovich distance between positive measures,” *Inventiones mathematicae*, vol. 211, no. 3, pp. 969–1117, 2018.
- [63] M. Cuturi, “Sinkhorn distances: Lightspeed computation of optimal transport,” *Advances in neural information processing systems*, vol. 26, 2013.
- [64] P. A. Knight, “The sinkhorn–knopp algorithm: convergence and applications,” *SIAM Journal on Matrix Analysis and Applications*, vol. 30, no. 1, pp. 261–275, 2008.
- [65] L. Chizat, G. Peyré, B. Schmitzer, and F.-X. Vialard, “Scaling algorithms for unbalanced optimal transport problems,” *Mathematics of Computation*, vol. 87, no. 314, pp. 2563–2609, 2018.
- [66] X. Wang, Y. Chen, and W. Zhu, “A survey on curriculum learning,” *IEEE Transactions on Pattern Analysis and Machine Intelligence*, vol. 44, no. 9, pp. 4555–4576, 2021.
- [67] T. A. Samuli Laine, “Temporal ensembling for semi-supervised learning,” *International Conference on Learning Representations (ICLR)*, vol. 30, 2017.
- [68] A. Tarvainen and H. Valpola, “Mean teachers are better role models: Weight-averaged consistency targets improve semi-supervised deep learning results,” *Advances in neural information processing systems*, vol. 30, 2017.
- [69] L. A. Caffarelli and R. J. McCann, “Free boundaries in optimal transport and monge-ampere obstacle problems,” *Annals of mathematics*, pp. 673–730, 2010.
- [70] L. Chapel, M. Z. Alaya, and G. Gasso, “Partial optimal transport with applications on positive-unlabeled learning,” *Advances in Neural Information Processing Systems*, vol. 33, pp. 2903–2913, 2020.
- [71] S. Zhang, Z. Li, S. Yan, X. He, and J. Sun, “Distribution alignment: A unified framework for long-tail visual recognition,” in *Proceedings of the IEEE/CVF conference on computer vision and pattern recognition*, 2021, pp. 2361–2370.
- [72] A. Dosovitskiy, L. Beyer, A. Kolesnikov, D. Weissenborn, X. Zhai, T. Unterthiner, M. Dehghani, M. Minderer, G. Heigold, S. Gelly *et al.*, “An image is worth 16x16 words: Transformers for image recognition at scale,” in *International Conference on Learning Representations*, 2020.
- [73] J. Huang, S. Gong, and X. Zhu, “Deep semantic clustering by partition confidence maximisation,” in *Proceedings of IEEE Conference on Computer Vision and Pattern Recognition (CVPR)*, 2020.
- [74] I. M. Metaxas, G. Tzimiropoulos, and I. Patras, “Divclust: Controlling diversity in deep clustering,” in *Proceedings of the IEEE/CVF Conference on Computer Vision and Pattern Recognition*, 2023, pp. 3418–3428.
- [75] L. Van der Maaten and G. Hinton, “Visualizing data using t-sne,” *Journal of machine learning research*, vol. 9, no. 11, 2008.



Chuyu Zhang received the B.E. degree in the School of Electronic Information Engineering from Wuhan University, Wuhan, China, in 2020. He is currently pursuing the Ph.D. degree in computer science and technology at ShanghaiTech University, supervised by Prof. Xuming He. His research interests concern computer vision and machine learning.



Hui Ren is currently pursuing a B.E. degree in computer science and technology at ShanghaiTech University. He is an undergraduate research assistant in PLUS Lab at ShanghaiTech University, advised by Prof. Xuming He. His research interests involve machine learning and computer vision. Personal Website: <https://rheiyang.github.io>



Xuming He received the Ph.D. degree in computer science from the University of Toronto, Toronto, ON, Canada, in 2008. He held a Post-Doctoral position with the University of California at Los Angeles, Los Angeles, CA, USA, from 2008 to 2010. He was an Adjunct Research Fellow with The Australian National University, Canberra, ACT, Australia, from 2010 to 2016. He joined National ICT Australia, Canberra, where he was a Senior Researcher from 2013 to 2016. He is currently an Associate Professor with the

School of Information Science and Technology, ShanghaiTech University, Shanghai, China. His research interests include semantic image and video segmentation, 3-D scene understanding, visual motion analysis, and efficient inference and learning in structured models.